Molecular Engineering of Ruthenium(II) Complexes with (3-Polyamino)phenanthroline for Developing Reusable Optical Sensors for Cu(II) ions

Anton S Abel, Andrey V. Cheprakov, Alexei D. Averin, Irina P. Beletskaya, Michel Meyer, Stéphane Brandès, Myriam Laly, Alla G. Bessmertnykh-Lemeune, Séverinne Rigolet

Molecular Engineering of Ruthenium(II) Complexes with (3-Polyamino)phenanthroline for Developing Reusable Optical Sensors for Cu(II) ions

Anton S. Abel,[a,b]* Andrey V. Cheprakov,[a] Alexei D. Averin,[a,c] Irina P. Beletskaya,[a,c] Michel Meyer,[b] Stéphane Brandès,[b] Myriam Heydel,[b] Alla Bessmertnykh-Lemeune,[b,d]* and Séverinne Rigolet[e]

[a] Lomonosov Moscow State University, Department of Chemistry, 1-3, Leninskie Gory, Moscow, 119991, Russia. E-mail: antonabel@list.ru

[b] Institut de Chimie Moléculaire de l'Université de Bourgogne (ICMUB), UMR 6302, CNRS, Université Bourgogne–Franche-Comté, 9 avenue Alain Savary, BP 47870, 21078 Dijon Cedex, France

[c] Frumkin Institute of Physical Chemistry and Electrochemistry, Russian Academy of Sciences, Leninsky Pr. 31, Moscow, 119071, Russia

[d] ENS de Lyon, UMR 5182, CNRS, Université Claude Bernard Lyon 1, Laboratoire de Chimie, 69342 Lyon, France. E-mail: alla.lemeune@ens-lyon.fr

[e] Institut de Science des Matériaux de Mulhouse, UMR 7361, CNRS, Université de Haute-Alsace, 15 rue Jean Starcky, 68057 Mulhouse Cedex, France

Supporting information for this article is given via a link at the end of the document.

Abstract: This work is aimed at the development of synthetic approaches to luminescent hybrid organic-inorganic materials based on chemosensors bearing phosphonate anchoring groups for detection of toxic metal ions in aqueous solutions. To that end, sensing properties of phosphonate-substituted ruthenium(II) complex with (3-polyamino)phenanthroline **Ru(N_3P_3phen)** towards toxic metal ions in aqueous media at physiological pH were investigated and compared to those of known dual-channel (spectrophotometry and luminescence) selective chemosensor **Ru(N_2P_2phen)** for copper(II) ions. The **Ru(N_3P_3phen)** complex enables only to detect copper(II) by luminescence measurements and is more sensitive (limit of detection (LOD) is 0.02 μM) than **Ru(N_2P_2phen)**. The main advantage of the chemosensors **Ru(N_2P_2phen)** and **Ru(N_3P_3phen)** studied herein is the possibility to immobilize them on titanium oxide surfaces without extra-synthetic costs using phosphonate substituents as anchoring groups. After activation with TMSBr, both complexes were successfuly grafted on hydrated mesoporous TiO_2 (S_{BET} = 650 m^2/g) performing reactions in DMF solutions at room temperature. Strong covalent binding of chemosensors **Ru(N_2P_2phen)** and **Ru(N_3P_3phen)** to the mesoporous TiO_2 support provides high chemical stability to the functionalized solids **Ru(N_2P_2phen)@TiO_2** and

Ru(N$_3$P$_3$phen)@TiO$_2$ but only one of them gives an optical response in the presence of copper(II) ions. The **Ru(N$_3$P$_3$phen)@TiO$_2$** material thus prepared allows for the luminescent detection of cupric ions in aqueous solutions displaying LOD lower than 10^{-13} M. Such a high sensitivity is unprecedented and cannot be obtained using soluble chemosensors in solutions. This solid-state sensor can be regenerated and reused at least three times.

Introduction

The development of molecular-based optical methodologies for detection and quantification of various analytes has spurred tremendous research efforts.[1,2] This now mature field continues to attract an increasing amount of attention due to rapid instrumental progresses and steadily growing analytical demands in the field of biochemistry, medicinal chemistry, industrial production and environmental pollution monitoring.[3–7] In this context, special interest is devoted to the development of selective chemosensors and materials for transition metal ions detection, since some of these cations are used in trace amounts in biological processes by living matter, while at the same time they continue to be an environmental and health concern when their concentrations exceed critical levels.[8–10]

Major recent achievements in this field are related to the conception of chemosensors and nanosized sensing systems that change their light emitting properties in the presence of the target cations.[7,11–16] These detectors take advantage of the high sensitivity and versatility of photoluminescence spectroscopy. However, they commonly suffer from some drawbacks, such as slow response, poor chemical or photostability, irreversibility, short lifetimes, low solubility, and/or low quantum yields in aqueous media. Most of the recent works in this field are focused on the structural optimization of soluble chemosensors. At the same time cutting-edge developments in luminescence sensing in aqueous media mostly deal with interfacial nanoscale systems, which offers fast real-time and in situ analyses of environmental or biological samples without contaminating them, reusability of sensing devises, and sometimes opens way to achieve unusual and useful properties such as sequestration of toxic ions or specific selectivity.[17,18] To get access to such devices, the immobilization of chemosensors on a solid support is regarded as the most appealing strategy.[19,20] However, luminescent properties of organic compounds is known to be highly sensitive to the medium and chemical environment of the luminophore, thus restricting the number of suitable solid supports. From a synthetic point of view, this limited choice often imposes laborious structural modifications of the molecular probe in order to prepare a suitable precursor of the desired sensing material.

The stable and inert ruthenium tris(diimine) complexes incorporating bipyridine, terpyridine, or 1,10-phenanthroline ligands have been widely explored as luminophores in molecular recognition, because they display photoluminescence in the visible region of the electromagnetic spectrum, large Stokes

shifts, low toxicities and high chemical, thermal, and photostabilities.[21–24] These positively charged complexes exhibit a high brightness[25] in aqueous media that can be advantageously exploited for increasing both the selectivity and sensitivity of the molecular probes.[26,27] Moreover, these chemosensors are ideally suited for devising multiple-channel detectors allowing for example the simultaneous read-out of photoluminescence, light absorption, electrogenerated chemiluminescence, and redox signals.[28,29] Multiplexing is useful for performing multiple analyte detection but also for improving the selectivity and enlarging the dynamic concentration range for a specific analyte. Consequently, ruthenium tris(diimine) complexes have been widely used for labeling, sensing, or imaging gases (dioxygen,[30] nitric oxide,[31] and carbon monoxide[32]), biological analytes (DNA, sugars, methylglyoxal, thiols, or aminoacids),[33–36] and anions.[23,37] Most importantly, these positively charged ruthenium(II) complexes have also been implemented in highly-sensitive analytical protocols allowing for the quantification of toxic metal cations in biological and environmental samples by spectroscopic methods, not only in the visible but also in the NIR region.[29,38–45] Recently, we reported efficient synthetic strategy to prepare modular molecules containing ruthenium tris(diimine) complexes as a signaling group and phosphonate-substituted polyamine receptors which possess useful sensing properties.[46] Grafting of these compounds on solid support through phosphonate anchoring group could afford solid-state sensors which can be adapted for detection of various analytes varying the structure of polyamine receptors.

Immobilization of Ru^{2+} complexes was widely investigated for many practical applications,[47–50] but examples of sensing materials are rare, most of them were used for the detection of either gases or vapors.[30,51–57] The design of metal-ion sensing materials operating in aqueous media is tricky because of the hydrophilicity of charged Ru^{2+} complexes that promotes leaching into the aqueous phase, particularly after the uptake of the target cation. Moreover, the immobilized chemosensor may lose its emitting or sensing properties due to interactions with the solid support or to a less-efficient binding of the analyte.[58] In early works, immobilization of metal-ion chemosensors was mainly achieved by electropolymerization.[59–62] Another interesting example is the manufacturing of reusable optical devices based on titanium oxide films that exhibited selectivity for mercury(II) ions.[63–65] The covalent grafting of Ru^{2+} complexes through appended carboxylate anchoring groups was finally performed, because simple adsorption of the indicator on the surface of these TiO_2 films afforded materials of poor stability. For all these sensors, mercury(II) detection relied on the color change, while their emissive properties turned out to be less useful and were reported only for the non-grafted dyes.[65] Recently, hybrid photoluminescent sensing materials for Cu^{2+} ions were obtained by imbedding the ruthenium complexes bearing ligands with polar functional groups inside large-pore silica nanoparticles.[43] The tunnel structure of the silica support efficiently prevented the leaching of the chemisorbed dye. These hybrid

nanoparticles held promises for the in vivo Cu^{2+} detection, but their implementation into solid-state devices is more difficult.

In this work we investigated the preparation of a sensor prototype by covalent grafting of Ru^{2+} complexes on cheap mesoporous hydrated titanium(IV) oxide support using strong P–O–Ti bonding. Our recently published studies have shown that the phosphonate-substituted complex **Ru(N_2P_2phen)** (Figure 1) allows for selective dual-channel detection of the Cu^{2+} ion at physiological pH by monitoring simultaneously the absorption changes and the luminescence turn-off (ON–OFF probe) of the test solutions.[46] However, the LOD of copper(II), determined by spectrophotometry and fluorescence spectroscopy, was equal to 9 and 6 μM, that is rather high for chemosensors bearing this signaling group.[44,66–74] We assumed that this drawback can be overcome by increasing the number of donor sites in the receptor unit and prepared analogous complex **Ru(N_3P_3phen)** containing three phosphonate-substituted amide arms (Figure 1), investigated its sensing properties and grafted both chemosensors onto mesoporous amorphous titania to get insight into the influence of structural modifications of the receptor unit on selectivity and sensitivity of reusable molecular-based solid sensors thus obtained.

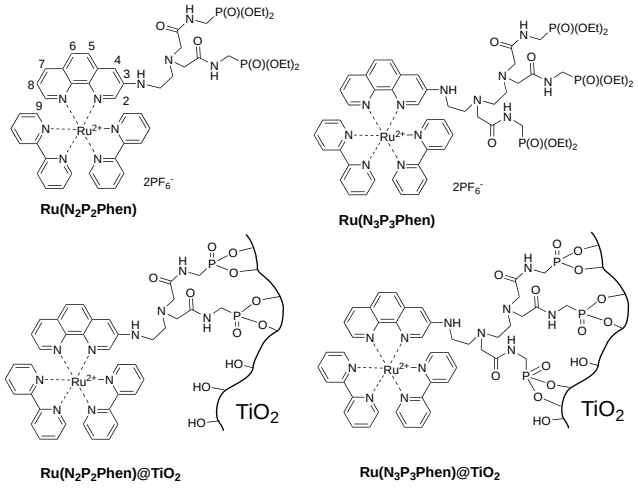

Figure 1. Structure of both studied molecular probes **Ru(N_2P_2phen)** and **Ru(N_3P_3phen)** and of the sensing materials **Ru(N_2P_2phen)@TiO_2**and **Ru(N_3P_3phen)@TiO_2**.

Despite extensive studies on Ru^{2+} complexes for sensing copper(II) ions in aqueous and physiologic media,[44,66–74] the sensing materials are limited to one example mentioned above.[43] Porous material **Ru(N_3P_3phen)@TiO_2** developed in this work is efficient for rapid and selective detection of Cu^{2+} ions in aqueous solutions. Careful optimization of the molecular precursor and the immobilization strategy

allows us to achieve unprecedent for luminescent sensors LOD in the detection of Cu^{2+} ions and reusability of the sensor.

Experimental

Materials and methods

Unless otherwise noted, all chemicals and starting materials were obtained commercially from Acros or Aldrich-Sigma Co. and used without further purification. [(2-Bromoacetylamino)methyl]phosphonic acid diethyl ester (**2**) was synthesized according to a known procedure.[75] The starting complex *cis*-$Ru(bpy)_2Cl_2$ was synthesized from $RuCl_3 \cdot 3H_2O$ according to a known method.[76] Mesoporous hydrated titanium(IV) oxide was obtained using a surfactant-free sol-gel procedure reported by us previously.[77] Preparative column chromatography was carried out using silica gel 60 (40–63 μm) from Merck Co. CH_2Cl_2 and CH_3CN were distilled over CaH_2, chloroform was distilled over P_2O_5.

^1H, ^{31}P, and ^{13}C NMR spectra were recorded with a Bruker Avance-400 MHz or a Bruker Avance III 500 MHz spectrometer in $CDCl_3$, CD_3OD, or CD_3CN, using the residual signals of $CHCl_3$, CHD_2OD or CHD_2CN as internal standards. The ^{31}P solid-state NMR experiments were performed at room temperature on a Bruker Avance II 300 spectrometer operating at B_0 = 7.04 T and equipped with a Bruker double channel 4 mm probe at a Larmor frequency of 121.47 MHz. The spectrum was recorded with a $\pi/2$ pulse duration of 4 μs and a recycling delay of 60 s at a spinning frequency of 14 kHz. ^{31}P spin-lattice relaxation times (T_1) was measured with the saturation-recovery pulse sequence. ^{31}P spectra were referenced to H_3PO_4 (85% in water). Spectral deconvolutions were performed using the Dmfit software (http://nmr.cemhti.cnrs-orleans.fr/dmfit/) with Gaussian/Lorentzian functions.

MALDI-TOF high-resolution mass-spectra (MALDI-TOF-HRMS) were obtained on a Bruker Daltonics Autoflex II and a Bruker Ultraflex II LRF 2000 mass-spectrometers and in positive ion mode with a dithranol matrix and polyethyleneglycols as internal standards. Accurate mass measurements (ESI-HRMS) were performed with a Thermo Scientific Orbitrap Elite high-field Orbitrap hybrid mass spectrometer. Microanalyses (CHN) were performed on a Thermo Electron Flash EA 1112 analyser. Ru, P, and Ti contents were measured after mineralization by inductively coupled plasma optical emission spectrometry (ICP-OES DUO) on an ICAP 7400 instrument from Thermo Scientific.

FT-IR spectra were registered either on a Nicolet iS 5 or a Bruker Vector 22 spectrophotometer. A micro-ATR accessory (Pike) was used in order to obtain FT-IR spectra of polycrystalline solid complexes.

UV–vis absorption and emission spectra were collected with an Agilent Cary 60 and a Horiba-Jobin-Yvon Fluoromax-2 spectrophotometer, respectively, using Suprasil 300 cuvettes (Hellma, l = 1 cm). Luminescence quantum yields were determined relative to $[Ru(bpy)_3](PF_6)_2$ in aerated acetonitrile according to a standard procedure.[78] The equation (1) was used to determine the relative fluorescence quantum yield:

$$\Phi_x = \Phi_{st} ((F_x \cdot A_{st} \cdot \eta_x^2)/(F_{st} \cdot A_x \cdot \eta_{st}^2)), \quad (1)$$

where A is the absorbance (in the range of 0.01–0.1), F is the area under the emission curve, η is the refractive index of the solvents (at 25 °C) used for the measurements, and the subscript x and st represents the compound under investigation and standard compound, respectively.

Emission spectra of the **Ru(N$_2$P$_2$phen)@TiO$_2$** and **Ru(N$_3$P$_3$phen)@TiO$_2$** materials were recorded using a Horiba-Jobin-Yvon FluoroMax-2 and FluoroMax-4 spectrofluorometers equipped with a support for solid samples and a KSPHERE-Petite integrating sphere from PTI, respectively. Diffuse reflectance spectra of the materials were acquired in the 200–800 nm range on a Carry 5000 (Agilent) UV–vis–NIR spectrophotometer outfitted with a praying Mantis™ accessory (Harrick). The baseline was recorded with a Spectralon® pellet used as standard. Corrected reflectance data (R) were converted to $f(R)$ values using the Kubelka–Munk function expressed as $f(R) = (1 – R^2)/2R$.

Nitrogen adsorption-desorption isotherms were measured with a BELSORP max analyzer (BEL Japan, INC.) at 77 K with samples degassed for 6 h at 80 °C under reduced pressure (10^{-5} torr). Specific surface areas (S_{BET}) were calculated according to the Brunauer–Emmett–Teller (BET) method.

Field-emission scanning electron microscopy (FESEM) images were collected with a Carl Zeiss Ultra Plus instrument.

Powder X-ray diffraction experiments were performed with an Empyrean diffractometer from the PANalytical company in the range $3° < 2\theta < 50°$, using a copper anticathode X-ray tube (Cu Kα_1 = 1.54060 Å and Cu Kα_2 = 1.54443 Å) and a X'Celerator detector outfitted with an anti-scattering slit of 5 mm. The uncrushed samples (few milligrams) were placed between two Mylar sheets and the analysis was performed in transmission mode using a focusing X-ray mirror equipped with fixed divergent and anti-scattering slits (aperture 0.5°) and 0.02 rad Soller slits.

All elemental analyses, solution NMR and FT-IR spectra and powder X-ray analyses were performed at the "Pôle Chimie Moléculaire", the technological platform for chemical analysis and molecular synthesis (http://www.wpcm.fr) of the Institut de Chimie Moléculaire de l'Université de Bourgogne and Welience™, a private subsidiary of the Université de Bourgogne.

Synthesis of chemosensors

The synthesis of N^1-(2-aminoethyl)-N^2-(1,10-phenanthrolin-3-yl)ethane-1,2-diamine (**1b**), **N_2P_2phen** and **Ru(N_2P_2phen)** was previously reported by us.[46]

Compound N_3P_3phen. A 15 mL flask equipped with a magnetic stirrer, a condenser and a gas outlet was charged with **1b** (70 mg, 0.25 mmol), chloroform (7 mL) and DIPEA (160 mg, 1.23 mmol). [(2-bromoacetylamino)methyl]phosphonic acid diethyl ester **2** (239 mg, 0.83 mmol) was added, and the reaction mixture was stirred at 40 °C for 48 h under argon. The solution was evaporated under reduced pressure and the residue was chromatographed on silica gel using pure CH_2Cl_2, and then CH_2Cl_2/MeOH (200:1 to 3:1 *v/v*) as eluents. Yield: 108 mg (48%); brown oil. FT-IR (cm^{-1}): 3270, 3049, 2981, 2910, 2826, 1669, 1605, 1589, 1530, 1477, 1443, 1423, 1390, 1299, 1224, 1162, 1099, 1022, 972, 830, 781, 732, 717, 576, 533, 483, 431. ^{1}H NMR (400 MHz, $CDCl_3$): δ = 1.25–1.35 (m, 18H, CH_3), 2.60–2.90 (m, 6H, CH_2N), 3.05–3.20 (m, 6H, $CH_2C(O)$), 3.33 (t, ^3J = 4.75 Hz, 2H, CH_2N), 3.65–3.80 (m, 6H, $CH_2P(O)$), 4.07–4.20 (m, 12H, CH_2OP), 7.13 (d, ^4J = 2.2 Hz, 1H, H4(Phen)), 7.47 (dd, ^3J = 8.0 Hz, ^3J = 4.4 Hz, 1H, H8(Phen)), 7.61 (d, ^3J = 8.8 Hz, 1H, H5(Phen)), 7.66 (d, ^3J = 8.8 Hz, 1H, H6(Phen)), 8.15 (dd, ^3J = 7.2 Hz, 1H, H7(Phen)), 8.50 (br. t, ^3J = 5.7 Hz, 2H, C(O)NH), 8.57 (br. t, ^3J = 5.7 Hz, 1H, C(O)NH), 8.83 (d, ^4J = 2.2 Hz, 1H, H2(Phen)), 9.06 (dd, ^3J = 4.4 Hz, ^4J = 1.8 Hz, 1H, H9(Phen)). NH-proton was not unambiguously assigned. ^{13}C NMR (100.6 MHz, $CDCl_3$): δ = 16.3 (d, $^3J_{PC}$ = 5.9 Hz, 6C, CH_3), 34.0 (d, $^1J_{PC}$ = 156.0 Hz, 1C, $CH_2P(O)$), 34.3 (d, $^1J_{PC}$ = 156.0 Hz, 2C, $CH_2P(O)$), 40.6 (1C, CH_2N), 52.4 (1C, CH_2N), 53.1 (1C, CH_2N), 54.1 (1C, CH_2N), 57.5 (1C, $\underline{C}H_2C(O)$), 58.5 (2C, $\underline{C}H_2C(O)$), 62.6 (d, $^2J_{PC}$ = 6.6 Hz, 4C, CH_2OP), 62.7 (d, $^2J_{PC}$ = 6.6 Hz, 2C, CH_2OP), 111.3 (1C), 121.0 (1C), 126.2 (1C), 126.3 (1C), 126.5 (1C), 130.2 (1C), 135.8 (1C), 137.5 (1C), 141.4 (1C), 144.3 (1C), 146.5 (1C), 149.8 (1C), 170.0 (2C, C(O)), 170.8 (1C, C(O)). ^{31}P NMR (162.5 MHz, $CDCl_3$): δ = 23.5 (2P), 23.6 (1P). MALDI-TOF-HRMS: *m/z* calcd for $C_{37}H_{62}N_8O_{12}P_3$: 903.3700 $[M+H]^+$; found: 903.3658.

Complex Ru(N_3P_3phen). A two-neck flask equipped with a magnetic stirrer and a reflux condenser was charged with *cis*-Ru(bpy)$_2$Cl$_2$ (38 mg, 0.078 mmol), **N_3P_3phen** (78 mg, 0.086 mmol) and 2 mL MeOH. The reaction mixture was refluxed for 20 h in the dark. The hot reaction mixture was passed through a glass filter and cooled down to r. t.. A saturated aqueous solution of NH_4PF_6 (0.3 mL) was added to this filtrate. After 5 min, the solution was diluted with distilled water (15 mL). The product was extracted by CH_2Cl_2 (3 × 20 mL) and the combined organic phases were dried over 3 Å molecular sieves. Then, the solution was evaporated under reduced pressure and the residue was chromatographed on silica gel using pure CH_2Cl_2, and then CH_2Cl_2/MeOH (50:1 to 10:1 *v/v*) as eluents. After chromatography, the product was dissolved in CH_2Cl_2 (20 mL), washed with distilled water (3 × 20

mL) to eliminate an excess of NH_4PF_6, and dried over 3 Å molecular sieves. Then the solution was evaporated under reduced pressure. Yield: 107 mg (86%); red glassy compound. FT-IR (cm^{-1}): 3316, 3299, 3286, 3265, 3084, 2980, 2931, 2650, 2372, 2344, 2323, 2288, 2187, 2167, 2140, 2110, 2081, 2051, 1981, 1919, 1668, 1600, 1532, 1466, 1445, 1392, 1369, 1301, 1218, 1162, 1100, 1021, 975, 876, 831, 764, 731, 718, 660, 648, 585, 555. ^{1}H NMR (400 MHz, CD_3CN): δ = 1.19–1.27 (m, 18H, CH_3), 2.64 (br. s, 4H, CH_2N), 2.72 (br. s, 2H, CH_2N), 3.05–3.25 (m, 8H, CH_2N, $CH_2C(O)$), 3.50–3.75 (m, 6H, $CH_2P(O)$), 3.95–4.10 (m, 12H, CH_2OP), 6.32 (br. s, 1H, NHPhen), 7.25 (ddd, ^3J = 7.4 Hz, ^3J = 5.8 Hz, ^4J = 1.2 Hz, 1H, H(bpy)), 7.31 (ddd, ^3J = 7.5 Hz, ^3J = 5.7 Hz, ^4J = 1.3 Hz, 1H, H(bpy)), 7.39–7.45 (m, 1H, H(bpy)), 7.48–7.52 (m, 2H, H5(Phen), H6(Phen)), 7.54–7.57 (m, 1H, H(bpy)), 7.57 (d, 1H, ^4J = 2.3 Hz, H4(Phen)), 7.64–7.76 (m, 4H), 7.80–7.83 (m, 1H, H(bpy)), 7.84–7.87 (m, 2H), 7.93–8.10 (m, 6H), 8.43 (dd, ^3J = 8.1 Hz, ^4J = 1.2 Hz, 1H, H7(Phen)), 8.48 (d, ^3J = 8.4 Hz, 1H, H(bpy)), 8.50–8.56 (m, 3H). ^{31}P NMR (162.5 MHz, CD_3CN): δ = –144.5 (m, $^1J_{PF}$ =706.5 Hz, 2P, PF_6^-), 22.0 (2P, $P(O)(OEt)_2$), 22.1 (1P, $P(O)(OEt)_2$). UV–Vis (H_2O, pH = 7.4): λ_{max} (ε, cm^{-1} M^{-1}) = 450 (10000), 354 (17000), 285 (53000) nm. Fluorescence (H_2O, pH = 7.4, λ_{ex} = 450 nm): λ_{em} = 603 nm. ESI-HRMS: *m*/*z* calcd for $C_{57}H_{77}N_{12}O_{12}P_3Ru$: 1316.4029 $[M–2PF_6]^{2+}$; found: 1316.4009.

Protonation Studies

Protonation and complexation studies were performed at room temperature. The solutions were prepared with double-deionized high-purity water (18.2 MΩ cm) obtained from a Millipore Simplicity apparatus. Solution concentrations and other experimental conditions are given in the corresponding figures. Protonation studies were conducted in a glass beaker equipped with magnetic stirrer and a LE438 combined pH-electrode fitted to a Mettler Toledo pH-meter by adding HCl (0.1 M or 0.01 M) or KOH (0.1 M or 0.01 M) to the solutions of **Ru(N$_3$P$_3$phen)**. Numerical data fitting of spectrophotometric titration curves was performed using the HypSpec program (Figures S2–S4 and S8–S11).[79,80] Distribution diagrams and electronic absorption spectra of **Ru(N$_3$P$_3$phen)** and its monoprotonated form calculated using the HypSpec program are shown in Figure S4.

Complexation of metal ions

Metal-binding experiments were conducted by a manual addition of the aliquots of metal salt solutions by a Hamilton syringe to a solution of **Ru(N$_3$P$_3$phen)** placed in a quartz cuvette. All metal salts used were perchlorates of general $M(ClO_4)n{\cdot}xH_2O$ formula. *Caution: although no problems were experienced, perchlorate salts are potentially explosive when combined with organic ligands and should be manipulated with care and used only in very small quantities.*

The $Hg(ClO_4)_2$ solution was prepared in acetonitrile (HPLC, Merck) to avoid hydrol-ysis of the salt. Aqueous solutions of metal perchlorates were prepared with concentra- tions approximately 1000-fold

of that of the ligands in order to decrease the influence of the medium changes on the spectra of the studied solutions. The isosbestic point observed in the UV–vis titration curves suggests that only one spectrally distinct complex was formed in the solution (Figure S10).Stability constants were calculated using nonlinear least squares analysis by means of HYPERQUAD software[80] after factor analysis of the combined data sets.[81] Numerical data processing was performed for both titrations with the HypSpec program, by taking into account the hydrolysis of copper(II).

The goodness of fit was assessed through the scaled standard deviation of the residuals (s), which has an expectation value of unity in the absence of systematic errors assuming a correct weighting scheme and by the physical significance of the calculated molar extinction coefficients. The results were checked by plotting calculated molar extinction graphs (Figure S11). The calculated absorption and emission spectra, together with distribution diagrams of **Ru(N_3P_3phen)** and of the copper complex are shown in Figures S9 and S11. The LOD for soluble sensors were determined by photoluminescence measurements using the 3σ-method.[82].

DFT calculations

The structures of bimetallic complexes Cu^{2+}/Ru(N_3P_3phen) and Zn^{2+}/Ru(N_3P_3phen) complexes were modelled by DFT calculations using Firefly quantum chemistry package,[83] which is partially based on the GAMESS (US)[84] source code. The calculations were performed using B3LYP functional with STO 6-31G(d,p) basis set for all elements except Ru, for which we have used the Stuttgart relativistic small-core effective core potential basis set.[85] The structure was assembled in a stepwise way, first by embedding the metal ion in the aminoethyl residue connected to the ruthenium core in order to form the starting 5-membered chelate ring. After full optimization, the coordination sphere of copper was completed by closing one by one additional chelate rings, while considering all possible isomers. The most stable arrangements were selected *via* a full geometry optimization. We believe that such a stepwise procedure reflects, at least in part, the real binding process of multiple chelation in solution. At the final stage, we involved the phosphonate residues. In doing so we have arrived at several isomeric structures, for which we have performed full optimization with increased precision and calculation of vibrational modes. Unfortunately, we came across several negative vibration frequencies for the final structure of the copper complex. Therefore, we have decided to withdraw the results for copper complex and used instead the results for zinc complex, exhibiting an almost identical geometry (Figure 7 and S15).

It is worth to note that such calculation definitely has nothing to do with real complexation in aqueous solutions, and there is no way to computationally estimate the equilibrium constants.

Synthesis of materials Ru(N_2P_2phen) or Ru(N_3P_3phen)

*General procedure***.** A dry Schlenk tube was charged with diethyl phosphonate esters **Ru(N_2P_2phen)** or **Ru(N_3P_3phen)** and dry CH_2Cl_2 (*c* = 0.1 M) under argon. Then, TMSBr (6 equiv. for each diethoxyphosphoryl group) was added *via* a syringe and the resulting mixture was stirred at r. t. for 24–48 h in the dark. Evaporation of volatiles under reduced pressure afforded the corresponding silyl phosphonate esters in quantitative yield. Then, 2.5 mL of dry DMF were introduced into the Schlenk tube with a syringe, followed by the addition of 60 equiv. of mesoporous hydrated TiO_2 under an argon stream. The suspension was stirred for 48 h at r. t. in the dark. The solid was collected by centrifugation, thoroughly washed with DMF (15 mL), water (15 mL), EtOH (3 × 15 mL), and ether (2 × 15 mL). The material was finally dried for 24 h at 80 °C under reduced pressure (2 mmHg).

Ru(N_2P_2phen)@TiO_2. The material was prepared according to the general procedure from 52 mg (0.038 mmol) **Ru(N_2P_2phen)**, 61 µL (0.46 mmol) TMSBr, and 244 mg mesoporous hydrated titania (2.30 mmol). Yield 162 mg. The elemental analysis of the solid is reported in Tables S1 and S2.

Ru(N_3P_3phen)@TiO_2. The material was prepared according to the general procedure from 60 mg (0.037 mmol) **Ru(N_3P_3phen)**, 89 µL (0.67 mmol) TMSBr, and 238 mg mesoporous hydrated titania (2.24 mmol). Yield 152 mg. The elemental analysis of the solid is reported in Tables S1 and S2.

Studies of complexation of toxic metal ions by the Ru(N_2P_2phen) or Ru(N_3P_3phen) materials

All metal salts used were perchlorates of general $M(ClO_4)n{\cdot}xH_2O$ formula. The $Hg(ClO_4)_2$ solution was prepared in acetonitrile (HPLC, Merck) to avoid hydrolysis of the salt. Aqueous solutions of metal perchlorates were prepared with concentrations approximately 1000-fold of that of the immobilized chemosensors in order to decrease the influence of the medium changes on the spectra of the studied solutions. Metal-binding experiments were conducted by a manual addition of the aliquots of metal salt solutions by a Hamilton syringe to a stirred suspensions of materials in deionized water placed in a quartz cuvette. Solution concentrations and other experiment conditions are given in the corresponding figures. After 2 min the samples were evaluated by photoluminescence spectroscopy.

LOD of copper(II) ions was determined by successive cascade dilutions of the analyzed sample a standard laboratory fluorimeter equipped with single monochromators and a 150 W Xenon lamp (Fluoromax-2 from Horiba-Jobin-Yvon).

Sorption properties of **Ru(N_3P_3phen)@TiO_2** were investigated adding aqeous solution of copper(II) complexes to a stirred suspencion of **Ru(N_3P_3phen)@TiO_2** in deionized water. Experimental

conditions are listed in Table S3. After stirring for 15 min the material was separated by filtration through Nylon Syringe Filter (0.22 μm) and investigated by ICP-OES.

In the recovering experiments the sample was centrifugated (Hettich Universal 320, 3500 rpm) to eliminate the supernatant. The recovered solid was thoroughly washed with a 10^{-3} M solution of Na_2H_2EDTA stirring the suspension for 10 min, centrifugates and then washed by deionized water and centrifugated. The solid thus obtained was then reused in the next analysis (Figure S22).

Results and Discussion

Synthesis

The molecular probes **Ru(N$_2$P$_2$phen)** and **Ru(N$_3$P$_3$phen)** were obtained from 3-bromo-1,10-phenanthroline according to a three-step reaction sequence developed by us previously.[46] As it can be seen from Scheme 1, the phosphonate-substituted ligands **N$_2$P$_2$phen** and **N$_3$P$_3$phen** were prepared by the *N*-alkylation of the polyamines **1a** and **1b** by diethyl[(2-bromoacetylamino)methyl]phosphonate (**2**). Despite the increased number of reactive centers in the chelator **1b,** the overall product yield was similar in both reactions. The complexation of the 1,10-phenanthroline chelators **N$_2$P$_2$phen** and **N$_3$P$_3$phen** by *cis*-Ru(bpy)$_2$Cl$_2$ in refluxing methanol afforded in high yields the target complexes which were isolated as hexafluorophosphonate salts.

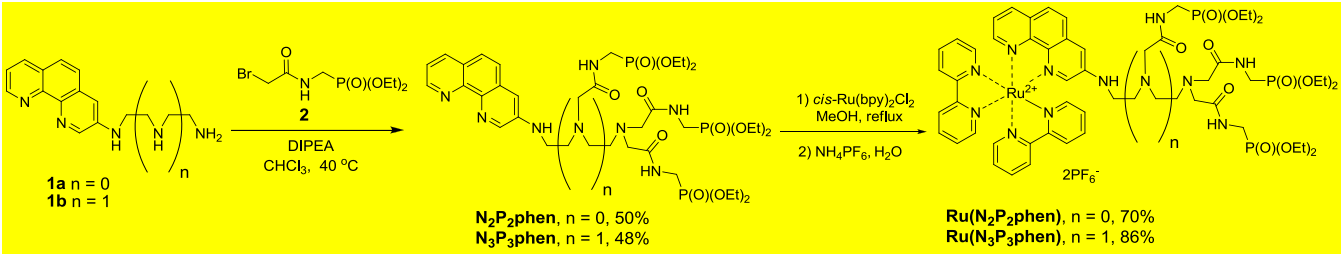

Scheme 1. Synthesis of chemosensors **Ru(N$_2$P$_2$phen)** and **Ru(N$_3$P$_3$phen)**.

Spectroscopic properties and protonation studies

Ru(N$_2$P$_2$phen) and **Ru(N$_3$P$_3$phen)** are soluble in water at pH 0.5–12 and in 0.03 M HEPES solution under physiological conditions (pH = 7.4). Their spectroscopic data are summarized in Table 1.

Table 1. Photophysical data and apparent protonation constants or pKa for **Ru(N_2P_2phen)** and **Ru(N_3P_3phen)**.

Complex	λ_{abs}, nm (log ε)[a]	λ_{em}, nm[b]	Φ[c]	Brightness, B, $M^{-1}\,cm^{-1}$ [d]	pKa[e]
Ru(N_2P_2phen)	285 350 450 (4.10)	(4.82)601 (4.30)	0.033[f]	415	2.02(1)[f]
Ru(N_3P_3phen)	285 350 450 (4.00)	(4.72)601 (4.23)	0.037	370	4.40(3)

[a] In 0.03 M HEPES solutions (pH = 7.4). Molar extinction coefficient (ε) is expressed in $M^{-1}\,cm^{-1}$. [b] λ_{ex} = 450 nm. [c] Quantum yields were determined in 0.03 M HEPES aerated solutions (pH = 7.4) using $[Ru(bpy)_3]^{2+}$ in aerated acetonitrile (Φ = 3.2%) as a standard (λ_{ex} = 450 nm).[86] [d] $B = \Phi(\lambda) \times \varepsilon(\lambda)$.[25] λ_{ex} = 450 nm [e] UV–vis spectrophotometric measurements. I = 0.1 M KCl, T = 298.2(2) K. [f] Reference [46].

The electronic absorption spectra of both compounds are similar and typical for $[Ru(bpy)_2L]$-type complexes (L = ligand). The most intense bands occurring in the 250–300 nm range were ascribed to π-π^* ligand-centered electronic transitions.[87,88] The spectra also display characteristic broad absorption bands in the visible region resulting from overlapping interligand bpy/phen-based charge transfer (LLCT) and spin-allowed metal–ligand charge transfer (MLCT) transitions typical for unsymmetrical heteroleptic Ru^{2+} complexes.[22] An additional absorption maximum appearing in the 300–380 nm region presumably corresponds to ligand–ligand π-π^* transitions involving bipyridine and phenanthroline ligands.[89] Interestingly, only this band progressively blue-shifted from 350 to 346 nm upon gradual addition of hydrochloric acid, as shown in Figure S1. Protonation studies and sensing properties of **Ru(N_2P_2phen)** were reported by us recently.[46] The protonation of **Ru(N_3P_3phen)** occurs in a significantly different pH range (Table 1) in full agreement with the expected higher basicity of nitrogen atoms bearing only one instead of two electron-withdrawing substituents. Nevertheless, at physiological pH both compounds exist in nonprotonated form.

Like many related ruthenium complexes,[21] **Ru(N_2P_2phen)** and **Ru(N_3P_3phen)** are bright luminophores. In aerated HEPES solutions, the emission spectrum for each complex shows a broad band covering the ca. 500–700 nm range with a maximum at 601 nm. The luminescence quantum yields of 0.033 and 0.037 for **Ru(N_2P_2phen)** and **Ru(N_3P_3phen)**, respectively, are roughly the same as that reported elsewhere for the parent $[Ru(bpy)_3]^{2+}$ chromophore in aqueous media (0.042).[21] Noteworthy, the emission spectra of both compounds are essentially pH insensitive over a wide range (pH = 0.5–10) (Figure S5), this can be explained by the lack of efficient photoinduced electron transfer (PET) process

between the aliphatic polyamine substituent and the ruthenium-based luminophore, as already reported for aliphatic amines and ruthenium polypyridyl complexes.[90]

Thus, **Ru(N$_3$P$_3$phen)** and **Ru(N$_2$P$_2$phen)** can be considered as a suitable dyes for spectroscopic monitoring of various analytes due to their high solubility and brightness in aqueous media. The low basicity of these compounds is favorable for sensing metal ions at physiological pH (pH = 7.4), avoiding the competitive protonation of the ionophore under nearly neutral conditions.

Detection of metal cations in solution

The sensing properties of **Ru(N$_3$P$_3$phen)** have been evaluated at a constant pH of 7.4 in HEPES buffered (c = 0.03 M) aqueous solutions and compared to those of **Ru(N$_2$P$_2$phen)**. Firstly, UV–vis absorption and emission spectra were recorded before and after the addition of 2 equivalents of 18 different metal (Li^+, Na^+, K^+, Mg^{2+}, Ca^{2+}, Sr^{2+}, Ba^{2+}, Mn^{2+}, Fe^{2+}, Co^{2+}, Ni^{2+}, Cu^{2+}, Zn^{2+}, Ag^+, Cd^{2+}, Hg^{2+}, Pb^{2+}, Al^{3+}, Cr^{3+}) perchlorate salts to the same **Ru(N$_3$P$_3$phen)** solution (Figures 2 and S6). The sensing properties of **Ru(N$_3$P$_3$phen)** slightly differ from those of **Ru(N$_2$P$_2$phen)**. Indeed, complex **Ru(N$_2$P$_2$phen)** allows for dual-channel (spectrophotometric and luminescence) selective detection of Cu^{2+} ions in the presence of other toxic metal ions. The metal-induced changes of the UV–vis absorption band shapes for **Ru(N$_3$P$_3$phen)** are observed only in the presence of copper(II) ions but are by far too small for any practical application. Fortunately, coordination of Cu^{2+} cations produces significant (80%) quenching of the emission band (Figures 2 and S7). Likewise, the response is fast and specific to copper, as shown by cross-selectivity experiments in which 2 equivalents of Cu^{2+} were added to pre-incubated solutions containing **Ru(N$_3$P$_3$phen)** and various mixtures of other metal ions (1 equiv.), such as Na^+, K^+, Mg^{2+}, Ca^{2+}, Ba^{2+}, Co^{2+}, Ni^{2+}, Zn^{2+}, Ag^+, Cd^{2+}, Hg^{2+}, Pb^{2+}, and Al^{3+} (Figure 2). In all cases, the luminescent response of **Ru(N$_3$P$_3$phen)** was very similar, suggesting that the receptor binds Cu^{2+} ions more strongly than any other tested metal.

The stability constant of the copper complex with **Ru(N$_3$P$_3$phen)** was determined both by absorption and luminescence spectrophotometry (Figures S8–11). The best fits were obtained when both data sets were modeled by a single equilibrium involving the formation of the 1:1 {Cu[**Ru(N$_3$P$_3$phen)**]}$^{4+}$ species with log K_{11} = 6.05(5) and 5.97(2), respectively. As can be seen from Table 1, the increase of donor sites in **Ru(N$_3$P$_3$phen)** as compared to **Ru(N$_2$P$_2$phen)** allows for significant stabilization of copper(II) complex.

As expected, the LOD of 0.02 µM determined by photoluminescence measurements using the 3σ-method[82] is remarkably lower (by approximately of two order of magnitude) than the one previously found for **Ru(N$_2$P$_2$phen)**, while similar LOD's have been reported for the best [Ru(diimine–ionophore)(diimine)$_2$] conjugates.[44,66,67,70–74]

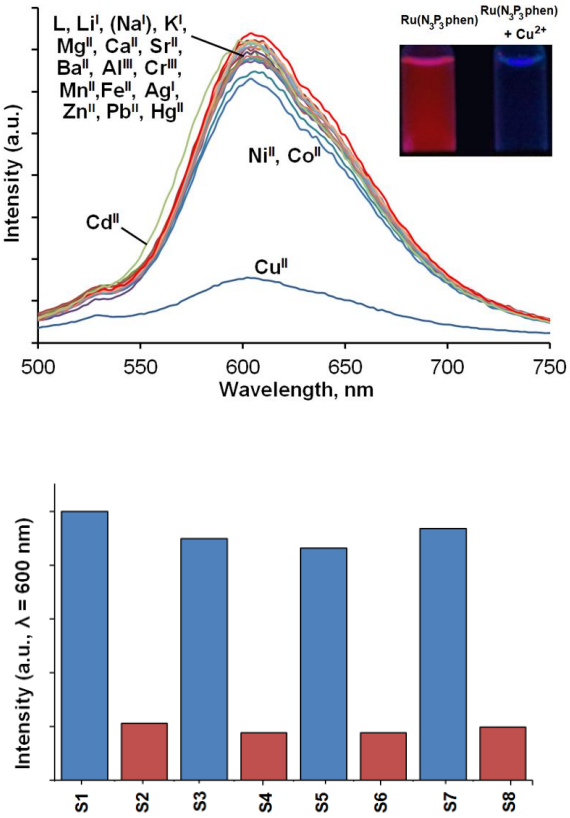

Figure 2. Fluorescence spectra of **Ru(N$_3$P$_3$phen)** before and after addition of 2 equiv. of metal perchlorates (top) and cross-selectivity studies of metal ion recognition by the sensor (bottom). The bar chart illustrates the emission intensity changes of a **Ru(N$_3$P$_3$phen)** solution before (blue) and after addition of 2 equiv. of Cu^{2+} (red). Initial sample composition: pure dye (S1); 1 equiv. of Li^{+}, (Na^{+}), K^{+}, Mg^{2+}, Ca^{2+}, Ba^{2+}, and Al^{3+} (S3); 1 equiv. of Mn^{2+}, Co^{2+}, Ni^{2+}, and Zn^{2+} (S5); 1 equiv. of Ag^{+}, Hg^{2+}, Cd^{2+}, and Pb^{2+} (S7); [**Ru(N$_3$P$_3$phen)**] = 4.7 μM, pH = 7.4, [HEPES] = 0.03 M, λ_{ex} = 450 nm.

To better understand the selectivity towards copper, the structure of **Ru(N$_3$P$_3$phen)** metal complex have been investigated combining UV–vis, FTIR, and ESI-HRMS analyses of the complex with DFT calculations. Firstly, **Ru(N$_3$P$_3$phen)** were reacted with one equivalent of $Cu(ClO_4)_2$ in methanol, and the residues obtained after evaporation of the solvent to dryness were characterized by ESI-HRMS and FT-IR spectroscopy.

ESI-HRMS signals corresponding to the [Cu[**Ru(N$_3$P$_3$phen)**] – 2H]$^{2+}$ and [Cu[**Ru(N$_3$P$_3$phen)**] + ClO_4 – H]$^{2+}$ species confirmed the formation of 1:1 copper adducts (Figure S12), in agreement with the results of titrations of **Ru(N$_3$P$_3$phen)** with copper(II) perchlorate in aqueous solutions.

Coordination mode of the amide groups was deduced from the comparison of FT-IR spectra recorded in the1500–1700 cm^{-1} region for {Cu[**Ru(N$_3$P$_3$phen)**]}$^{4+}$ and **Ru(N$_3$P$_3$phen)** (Figures S13–S14). It was reported that in copper(II)–amide complexes the amide I band appears in the 1615–1625 cm^{-1} region when the carbonyl oxygen atom is bound to the metal ion, whereas coordination of the deprotonated nitrogen atom (amidate binding mode) produces a red shift of the $\nu_{C=O}$ vibration mode down to ~1580

cm^{-1}.[91] In our case, the spectral interpretation is intricate owing to the overlapping of several other bands in this region. Nevertheless, we can safely conclude that the $\nu_{C=O}$ stretching modes appear in the 1635–1590 cm^{-1} region, indicating that most probably the oxygen atom of the amide group is coordinated to the metal center in both complexes.

Though FT-IR spectra of {Cu[**Ru(N_2P_2phen)**]}$^{4+}$ and {Cu[**Ru(N_3P_3phen)**]}$^{4+}$ are markedly similar, there is a significant difference in their UV–vis absorption spectra upon addition of Cu^{2+} ions to **Ru(N_2P_2phen)** and **Ru(N_3P_3phen)** solutions. A hypsochromic shift of the absorption maximum is significant only for **Ru(N_2P_2phen)**, which presumably indicates that the coordination of the aromatic nitrogen atom to Cu^{2+} in **Ru(N_3P_3phen)** is rather weak.

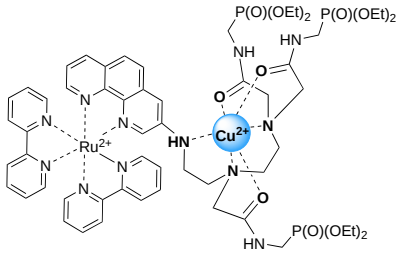

{Cu[Ru(N_3P_3phen)]}$^{4+}$

Figure 3. Schematic presentation of binding mode of **Ru(N_3P_3phen)** in coordination shell of copper(II) ion.

The higher stability of {Cu[**Ru(N_3P_3phen)**]}$^{4+}$ over {Cu[**Ru(N_2P_2phen)**]}$^{4+}$ is remarkable and likely accounted for by more favorable multiple chelation creating a better coordination environment for a cupric cation (Figure 3). Another probable rational is a larger separation between positive charges of metal centers in {Cu[**Ru(N_3P_3phen)**]}$^{4+}$, as compared to {Cu[**Ru(N_2P_2phen)**]}$^{4+}$.[92]

We also undertook a computational modelling of the molecular structure of complex {Cu[**Ru(N_3P_3phen)**]}$^{4+}$ mainly in order to understand whether such a manifold of binding sites connected *via* flexible linkers which is shown in Figure 3 can indeed be arranged in space in a meaningful and stable way around the metal ion to be detected. We were particularly interested in gaining an insight into two important issues: 1) whether the ruthenium complex unit might sterically interfere with binding zinc ion by multiple nitrogen coordination sites; 2) whether the geometry and flexibility of aminophosphonate residues might allow for the assembly of multi-chelate and how many coordination sites of incoming metal might thus be involved. The DFT computations were run using Firefly software, the standard B3LYP functional, and full-electron STO 6-31G(d,p) basis set for all atoms except Ru, for which we have used the Stuttgart relativistic small-core effective core potential basis set.[85] Unfortunately, we came across several negative vibration frequencies for the final structure of the copper complex, while the zinc homolog gave the required all-positive set of modes. Therefore, we have decided to withdraw the results for copper complex as being not fully compliant with the

requirements for finding a true energy minimum, and used instead the results for zinc complex, exhibiting an almost identical geometry (Figure 4 and S15). Both Zn^{2+} and Cu^{2+} ions are similar both by their size and coordination chemistry, thus we believe that such a study could be relevant for a rough modeling of the coordination mode of the new multidentate ligands.

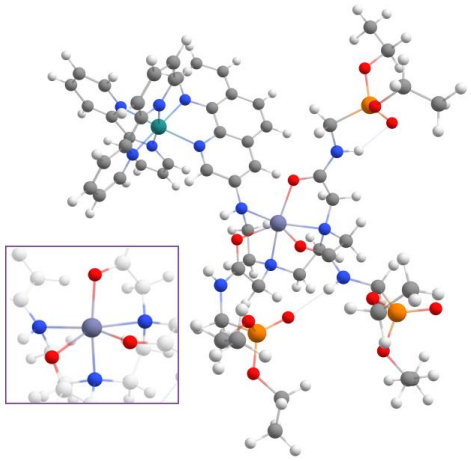

Figure 4. DFT calculated geometry of the bimetallic {Zn[**Ru(N_3P_3phen)**]}$^{4+}$ complex (DFT B3LYP/6-31G(d,p), see text for further details). The more stable *fac*-isomer is shown. Color code for the atoms: C (dark grey), H (light grey), N (blue), O (red), P (orange), Ru (green); Zn (violet).

The results of such modelling were indeed useful to demonstrate that three amino nitrogen atoms and three amido oxygen atoms were involved in the formation of complex giving a slightly distorted octahedral coordination of zinc ion. The very weak distortion of the ionophore backbone accounts for the low strain energy associated with the closure of five chelate rings in a *fac* arrangement. It should be noted that in the course of optimization, alternative spatial dispositions of the N_3O_3 donor set were tested, affording two *mer* and *fac* isomers characterized by very similar calculated formation energies, in agreement with the high flexibility of the binding arms and their ability to easily wrap around the six-coordinated metal center. As the geometry of the ruthenium chromophore and the interatomic Ru···Cu distances are most likely unaffected by the different layouts of the N_3O_3 atom set around the incoming Cu^{2+}, the emissive properties of the various isomers should be essentially indistinguishable from each other. At the other hand, such a variability would make the chelation and the assembly of full octahedral complex more favorable from the entropic point of view, as if allowing a certain degree of disorder in the process.

Thus, the computational modelling helped to ensure that such a sophisticated ligand involving a bulky ruthenium complex unit and a flexible array of extended chelating arms at its periphery, can indeed be quite competent in binding other cations. Moreover, we can safely infer from the quite large

intermetallic distance (> 7 Å) between two metal ions that Coulomb repulsion does not strongly imped metal uptake by the ionophore, especially in aqueous media having a huge dielectric constant. Thus, the formation of up to five chelate rings to achieve full octahedral coordination of copper and the low strain energy, most likely account for the better sensing performances of **Ru(N_3P_3phen)** over **Ru(N_2P_2phen)**, the latter offering only a N_2O_2 donor set and the possibility to create only three chelate rings.

The much higher affinity of both ligands for copper(II), as compared to other divalent cations under study, is in line with the Irving-Williams trend that predicts a stability increase among the first-raw transition metals in the order $Mn^{2+} < Fe^{2+} < Co^{2+} < Ni^{2+} < Cu^{2+} > Zn^{2+}$. Thus, in the presence of competing divalent metal ions, the preference for Cu^{2+} can be explained by a stronger ligand-field and Jahn-Teller stabilization energy, which outweighs the destabilization due to the presence of two cations.

Thus, while **Ru(N_2P_2phen)** can be considered as a dual-channel selective chemosensor for Cu^{2+}, [46] **Ru(N_3P_3phen)** is of interest too because of its higher sensitivity in case of luminescence measurements. With these two promising material precursors containing phosphonate anchoring groups in hand, we turned our efforts towards the fabrication of sensing materials.

Immobilization of chemosensors Ru(N_2P_2phen) and Ru(N_3P_3phen) on TiO_2

In view of obtaining reusable chemosensors for detecting toxic cations in environmental samples, both ruthenium complexes **Ru(N_2P_2phen)** and **Ru(N_3P_3phen)** were covalently bound to a chemically-stable solid support, namely TiO_2. Recent investigations of hybrid organic-inorganic materials based on phosphonates[93,94] revealed that metal oxides and polymeric phosphonate networks can be used as a solid support for heterogenization of transition metal complexes, including ruthenium tris(diimine) complexes.[95–104] However, to our knowledge, these materials have never been used in the development of luminescent sensors. The functional materials based on TiO_2 are cost-effective and display high thermal and chemical stability, stemming from the robustness of Ti–OP(O) and P–C bonds and the presumably multidentate coordination mode of the grafted phosphonate group. Both **Ru(N_2P_2phen)** and **Ru(N_3P_3phen)** are well suited for manufacturing such materials, since each molecule possesses several protected phosphonate anchoring groups located far away from the signaling unit that should contribute to the stability of the modified solid and minimize the influence of the support on the luminophore emission properties.

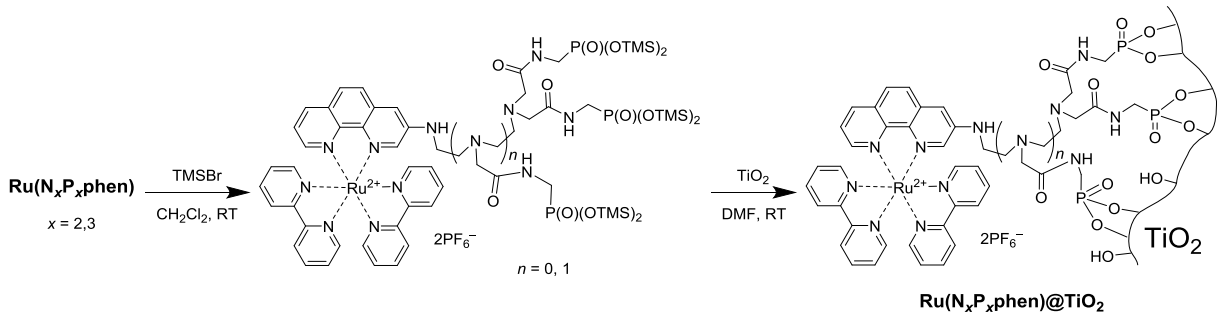

Scheme 2. Grafting of **Ru(N$_2$P$_2$phen)** and **Ru(N$_3$P$_3$phen)** on the surface of mesoporous TiO_2.

To explore the usefulness of this approach, **Ru(N$_2$P$_2$phen)** and **Ru(N$_3$P$_3$phen)** were grafted onto the surface of hydrated amorphous titanium oxide (Scheme 2), which does not exhibit any photocatalytic activity by its own. Such cost-effective mesoporous TiO_2 (S_{BET} = 650 m^2 g^{-1}) is readily available by a template-free sol-gel method.[77] To prepare the target materials we employed a sol-gel process in organic solvents,[105,106] since the immobilization of phosphonates in aqueous media occurs mainly through monodentate P–O–Ti interactions and thus yields less-stable materials.[107] Moreover, the possible occurrence of free phosphonate groups could be deleterious as these could strongly bind copper, displacing thereby some amido oxygen and/or amino nitrogen donor atoms and profoundly alter the sensing properties of **Ru(N$_2$P$_2$phen)** and **Ru(N$_3$P$_3$phen)**.

To enable the grafting process, the dialkyl phosphoester groups were first transformed into more reactive bis(trimethylsilyl)phosphonates by reacting in the dark **Ru(N$_2$P$_2$phen)** and **Ru(N$_3$P$_3$phen)** with TMSBr in CH_2Cl_2 at room temperature. These moisture-sensitive compounds were obtained in quantitative yields and engaged in the next step after evaporation of the reaction mixture to dryness. The residue was dissolved in dry DMF and the solution was added to mesoporous titania (the Ru/Ti molar ratio was 1:60) at room temperature in the dark. The empirical formulas of **Ru(N$_2$P$_2$phen)@TiO$_2$** and **Ru(N$_3$P$_3$phen)@TiO$_2$** were derived from the content of six elements (C, H, N, Ti, Ru, P) (Tables S1 and S2). The Ru/Ti ratio was found to be of 1:74 and 1:71, respectively, which is close to the theoretical values expected for complete grafting of the complexes (1:60).

N_2 adsorption–desorption isotherms of **Ru(N$_2$P$_2$phen)@TiO$_2$** and **Ru(N$_3$P$_3$phen)@TiO$_2$** at 77 K are presented in Figure 5. Upon the derivatization of TiO_2, no change in the shape of the isotherms was observed, whereas a marked decrease in the BET surface area (from 650 to 410 and 465 m^2 g^{-1}, respectively) was noted, which is consistent with the presence of a significant amount of grafted complexes on the surface. Powder X-ray diffraction measurements confirmed that the pristine mesoporous titania, **Ru(N$_2$P$_2$phen)@TiO$_2$** and **Ru(N$_3$P$_3$phen)@TiO$_2$** were all non-crystalline solids.

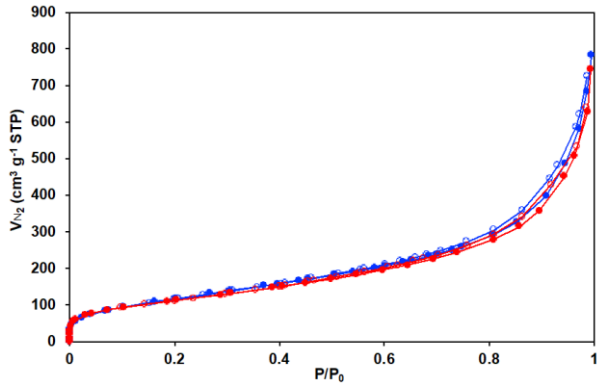

Figure 5. Nitrogen adsorption–desorption isotherms for **Ru(N_2P_2phen)@TiO_2** (blue lines and circles) and **Ru(N_3P_3phen)@TiO_2** (red line and circles) materials.

The morphology of **Ru(N_3P_3phen)@TiO_2** was studied by SEM and compared with that of the bare TiO_2 (Figure 6). The latter is composed of strongly aggregated nanoparticles of similar shape and quite narrow grain-size distribution. Grafting of **Ru(N_3P_3phen)** does not have any influence on the cauliflower-like morphology of the solid. The mesoporous nanospheroids with a diameter ranging from 5 to 20 nm, are irregularly distributed in the space and separated by large holes of hundreds of nanometers, thus providing a good accessibility to the bound receptors. This morphology is therefore perfectly suited for sensing purposes.

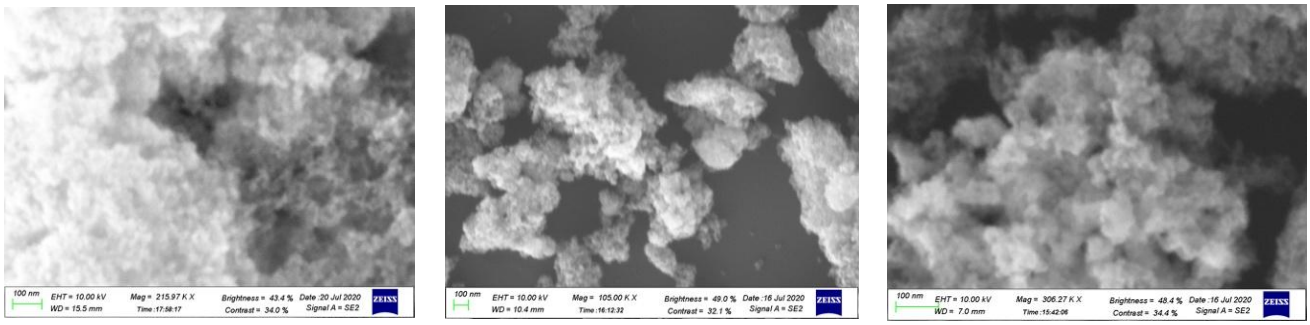

(a) **(b)** **(c)**

Figure 6. SEM microphotographs of (a) bare hydrated TiO_2, (b) **Ru(N_2P_2phen)@TiO_2**, and (c) **Ru(N_3P_3phen)@TiO_2**.

The intact structure of the immobilized complexes was proven by FT-IR and UV–vis diffuse reflectance spectroscopies. In brief, the spectral signatures of both ruthenium complexes before and after immobilization on TiO_2 were remarkably similar. In the FTIR spectra (Figures S18 and S19), vibration bands assigned to the heteroaromatic, amide, and phosphonate groups are all much weaker as compared to the Ti–OH and O–H stretching modes. It should be stressed that the chemosensor loading was intentionally kept rather low to avoid interferences between too closely lying neighboring units. Kubelka-Munk transformed UV–vis diffuse reflectance spectra of the studied solids show a strong and broad absorption feature in the high energy region (< 300 nm) as displayed on the top of Figure 7a for

Ru(N$_3$P$_3$phen)@TiO$_2$. This band was attributed to the TiO_2 phase. The spectral shape in the 350–550 nm range resembles closely to that observed for both **Ru(N$_2$P$_2$phen)** and **Ru(N$_3$P$_3$phen)** complexes by transmission in aqueous solutions, confirming that the chromophores keep their integrity after immobilization.

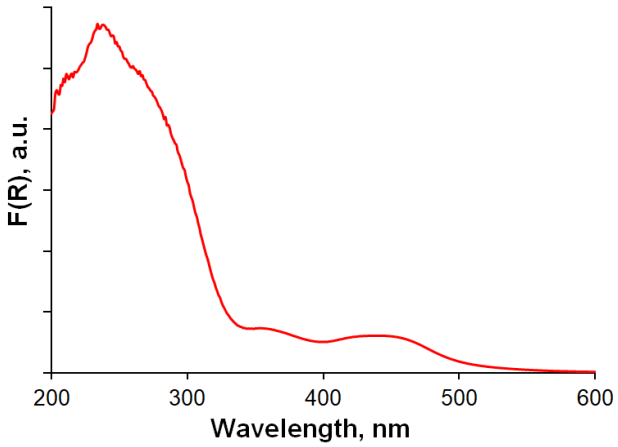

(a)

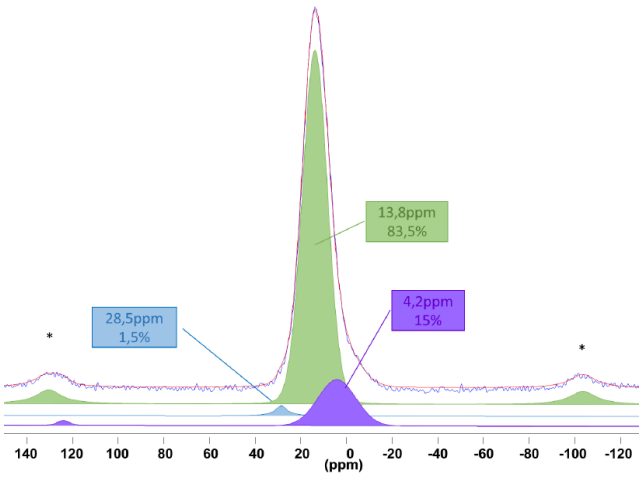

(b)

Figure 7. (a) Kubelka-Munk transformed diffusion reflectance spectrum (top) and overlay of the experimental (blue line) and simulated (red line). (b) ^{31}P MAS NMR spectrum (bottom) of **Ru(N$_3$P$_3$phen)@TiO$_2$**. Stars indicate spinning sidebands. Deconvoluted spectral components are shown in green, violet, and blue.

The ^{31}P MAS NMR spectrum of **Ru(N$_3$P$_3$phen)@TiO$_2$** is presented on the bottom of Figure 7b. A broad resonance at about 14 ppm indicates that C–P bonds were not cleaved during the grafting step, else signals of phosphates attached to amorphous titania would have been observed between –21 and –4 ppm.[106] For layered titanium phosphonate crystallites, a sharp phosphorus signal was observed at –4

ppm.[106] ^{31}P chemical shifts in the 10–30 ppm range are typical for well-isolated phosphonate molecules covalently bound to titania surface. As shown in Figure 8, the observed signal could be resolved into three components with maxima at 4.2 (15%), 13.8 (83.5%), and 28.5 ppm (1.5%). The low contribution of both lower and higher field signals indicates that more than 80% of the phosphonate anchoring groups are equivalent and bound to the surface in the same manner. The major signal (δ_P =13.8 ppm) is up-field shifted as compared to those of TiO_2-grafted alkylphosphonic acids,[108,109] presumably because of the magnetic anisotropy created by the carbonyl groups in the vicinity of the phosphorus atom. Unfortunately, the precise binding mode of phosphonate groups anchored to titania-based materials cannot be univocally deduced from chemical-shift correlations.[106–108] However, taking into account the high reactivity of phosphonic trimethylsilyl diesters and the report on the grafting of bis(trimethylsilyl) phenylphosphonates on TiO_2 surfaces,[106] it seems reasonable to assume that at least two oxygen atoms per phosphonate group are covalently anchored to the surface.

Both **Ru(N$_2$P$_2$phen)@TiO$_2$** and **Ru(N$_3$P$_3$phen)@TiO$_2$** solids were photoemissive, as shown in Figure S20. The powder spectra display asymmetric bands, with maxima at about 620 nm. Luminescence quantum yields of 0.5 and 0.4%, respectively, were determined with an integrating sphere.

Sensing properties of Ru(N$_2$P$_2$phen)@TiO$_2$ and Ru(N$_3$P$_3$phen)@TiO$_2$

The sensing properties of both materials suspended in aqueous solution were evaluated by photoluminescence spectroscopy, firstly by adding increasing amounts of copper perchlorate. Quenching was only observed for **Ru(N$_3$P$_3$phen)@TiO$_2$** (Figure 8a), while the emission band of **Ru(N$_2$P$_2$phen)@TiO$_2$** remained almost unaffected for copper concentrations reaching up to 10^{-3} M (Figure S21). The drastically reduced flexibility of the amidophosphonate arms once **Ru(N$_2$P$_2$phen)** was grafted, might explain the affinity loss for copper(II) and the almost disappearance of any detectable optical response. Thus, further studies exclusively were focused on **Ru(N$_3$P$_3$phen)@TiO$_2$**. The response time of that material was found to be shorter than 2 min, while the intensity of emitted light remained thereafter constant for at least 10 min. Contacting the solid with a 10^{-3} M copper solution in pure water reduced the luminescence intensity by a factor of 3. Successive cascade dilutions of the analyzed sample (Figure 8b) enabled to estimate a limit of detection better than 10^{-13} M by using a standard laboratory fluorimeter equipped with single monochromators and a 150 W Xenon lamp (Fluoromax-2 from Horiba-Jobin-Yvon). Such a high sensitivity cannot be obtained using soluble luminescent molecular probes but was achieved herein thanks to the chemisorption of Cu^{2+} on the functionalized solid. As shown in Figure 8c, filtration of sample through a membrane reveal that chemosensor didn't washed off in solution. Thus, **Ru(N$_3$P$_3$phen)@TiO$_2$** turns out to be an extremely appealing sensor and sequestering agent for ultra-purification of contaminated fluids.

As shown in Figure 9, competitive binding studies revealed that Cu^{2+} (10^{-4} M) could be effectively detected in the presence of other metal ions at the same individual concentration levels, including Li^{+}, Na^{+}, K^{+}, Mg^{2+}, Ca^{2+}, Ba^{2+}, Co^{2+}, Ni^{2+}, Zn^{2+}, Ag^{+}, Hg^{2+}, and Al^{3+}. Only Cd^{2+} and Pb^{2+} significantly diminished the luminescence response, presumably because of the sorption of these metal ions on the titania surface.

We also briefly investigated the sorption properties of the materials by analyzing the filtrates by ICP-OES. Results for **Ru(N$_3$P$_3$phen)@TiO$_2$** are summarized in Table 2 (see Table S3 for more details) and compared to those obtained with non-functionalized TiO_2. The hybrid material is more efficient than pristine TiO_2 for taking up copper(II). For a Cu/Ru molar ratio of 0.33, about 90% of the total copper is sorbed by the material. However, when the Cu/Ru molar ratio was increased up to 1.33, the uptake was much lower than expected as it reached only ~66%. Based on the difference between the measured and theoretical loadings, it can be inferred that about 33% of the anchored molecules are inaccessible to the analyte.

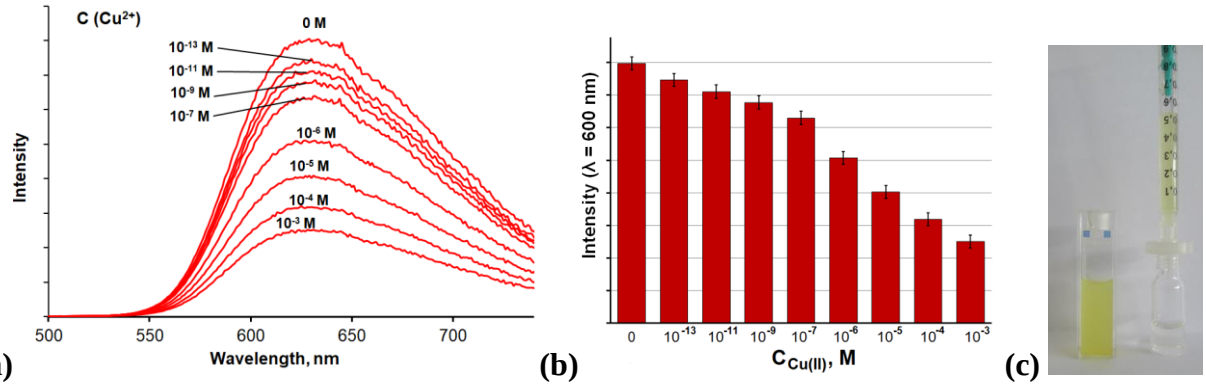

Figure 8. (a) Evolution of the photoluminescence spectrum of **Ru(N$_3$P$_3$phen)@TiO$_2$** suspended in water (λ_{ex} = 380 nm) in the presence of $Cu(ClO_4)_2$ (0–10^{-3} M) and (b) of the intensity of the light emitted at 600 nm. **(c)** Filtration of a **Ru(N$_3$P$_3$phen)@TiO$_2$** suspension leading to a colorless and non-emissive solution.

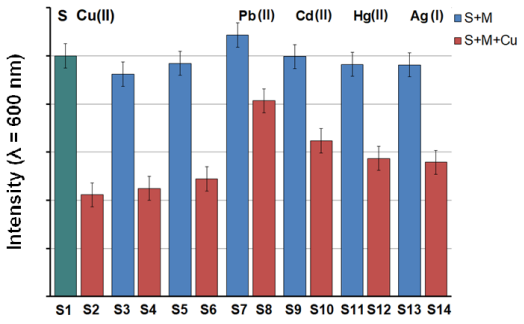

Figure 9. Cross-selectivity studies of metal ion recognition by **Ru(N$_3$P$_3$phen)@TiO$_2$** suspended in water (λ_{em} = 600 nm, λ_{ex} = 380 nm). The bar chart illustrates the emission intensity changes before (blue bars) and after addition of Cu^{2+} (c = 10^{-4} M, red bars). Initial sample composition: no added cation (S1, green bar); Li^+, Na^+, K^+, Mg^{2+}, Ca^{2+}, Ba^{2+}, and Al^{3+} (c = 10^{-4} M for each cation, S3); Mn^{2+}, Co^{2+}, Ni^{2+}, and Zn^{2+} (c = 10^{-4} M for each cation, S5); Pb^{2+} (c = 10^{-4} M, S7); Cd^{2+} (c = 10^{-4} M, S9); Hg^{2+} (c = 10^{-4} M, S11); Ag^+ (c = 10^{-4} M, S13).

Table 2. Sorption of Cu^{2+} by TiO_2 and **Ru(N$_3$P$_3$phen)@TiO$_2$**.[a]

Solid	Cu_{tot}/Ru molar ratio	m_{tot}(Cu) (µg)	[Cu] in solution (µg/L)	m(Cu) in solution (µg)	m(Cu) sorbed (µg)	Cu_{sor}/Ru (molar ratio)	Sorption of Cu (µg/mg)
TiO_2	-	102.5	7879.4	94.6	7.9	-	0.88
Ru(N$_3$P$_3$phen)@TiO$_2$	0.33	25.6	702.1	2.1	23.5	0.31	2.35
Ru(N$_3$P$_3$phen)@TiO$_2$	1.33	102.5	4371.8	52.5	50.0	0.66	5.00

[a] Cu^{2+} concentrations in the solution before and after sorption on the studied solids (15 min, r. t.) were determined by ICP-OES.

Finally, the recycling of the sensing material was investigated. After the first analysis, the suspension was centrifuged to eliminate the supernatant. The recovered solid was thoroughly washed with a 10^{-3} M solution of Na_2H_2EDTA followed by deionized water, and then reused in the next analysis (Figure S22). As shown in Figure 10, the sensor can be reused at least three times.

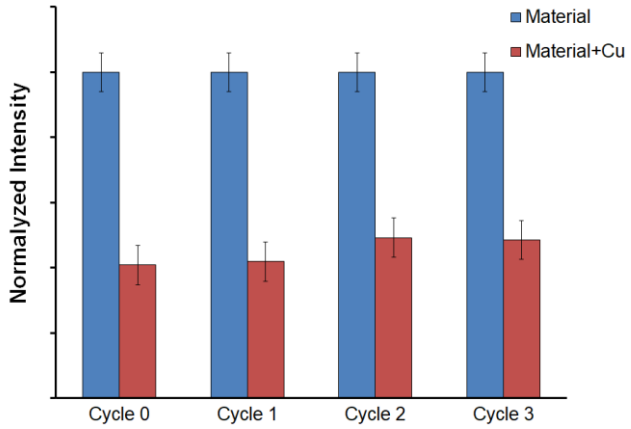

Figure 10. Recycling of **Ru(N$_3$P$_3$phen)@TiO$_2$** in the copper(II) detection assay. The bar chart illustrates the emission intensity changes of a **Ru(N$_3$P$_3$phen)@TiO$_2$** suspension in water before (blue) and after addition of Cu^{2+} (c = 10^{-4} M, red bars) for three subsequent cycles after regeneration. λ_{em} = 600 nm, λ_{ex} = 380 nm.

Conclusions

In this work we demonstrated that hybrid organic-inorganic materials prepared by grafting ruthenium(II) complexes with (3-polyamino)phenanthroline ligands onto porous titania surface through phosphonate anchoring group sare easily available and promising for detection of target analytes in aqueous media. As proof-of-conception studies we have developed a rapid, highly sensitive and

reusable photoluminescent sensing material for selective detection of toxic copper(II) ions in aqueous solutions.

To that end, phosphonate-substituted chemosensors **Ru(N_2P_2phen)** and **Ru(N_3P_3phen)** bearing ruthenium(II) complexes as a signaling group were prepared and investigated as molecular probes for toxic metal ions. We also developed an efficient procedure for immobilization of these chemosensors by treating them with TMSBr before grafting the obtained silyl esters onto mesoporous titanium oxide. Strong covalent binding of chemosensors **Ru(N_2P_2phen)** and **Ru(N_3P_3phen)** through Ti–O–P bonds to the mesoporous TiO_2 support provides a high chemical stability to the functionalized solids **Ru(N_2P_2phen)@TiO_2** and **Ru(N_3P_3phen)@TiO_2** thus obtained but only one of them gives an optical response on the presence of copper(II) ions in aqueous solutions. The **Ru(N_3P_3phen)@TiO_2** material allows for the selective luminescent detection of cupric ions displaying LOD lower than 10^{-13} M. Such a high sensitivity is unprecedented and cannot be obtained using soluble molecular probes in homogeneous solutions. The sensor can be used for real-time analysis without sample contamination and can be regenerated and reused several times.

Among possible applications, these materials could be used for example as a copper saturation indicator in water purification cartridges by simple visual inspection of a **Ru(N_3P_3phen)@TiO_2** layer packed at the outlet of the extraction column illuminated with a blue LED.

Acknowledgements

This work was supported by the Russian Foundation for Basic Research (RFBR grant no. 18-33-00279), the Centre National de la Recherche Scientifique (CNRS), the Conseil Régional de Bourgogne (PARI IME SMT8 and PARI II CDEA programs), the European Union (European Regional Development Fund, FEDER program). A. Abel is grateful to the French government and French embassy in Russia for a SSTE-2016 Grant. This work was carried out in the frame of the International Associated French–Russian Laboratory of Macrocycle Systems and Related Materials (LIA LAMREM, 2011–2019), jointly funded by the CNRS and the Russian Academy of Sciences (RAS).[52] Quentin Bonnin, Marie-José Penouilh, Diana Del Bianco, and Marcel Soustelle are warmly acknowledged for their technical support.

References

1. *Chemosensors: Principle, Strategies, and Applications*, eds. B. Wang and E. V. Anslyn, Wiley Series in Drug Discovery and Development, John Wiley & Sons, Inc. , Hoboken, 2011, 496 p.
2. *Chemosensors of Ion and Molecule Recognition*, eds. J. P. Desvergne and A. W. Czarnik, NATO ASI Series, Springer, Netherlands, 1997, 245 p.

3. *Frontiers in Chemical Sensors: Novel Principles and Techniques*, eds. G. Orellana and M. C. Moreno-Bondi, Springer Series on Chemical Sensors and Biosensors, Springer-Verlag Berlin, Heidelberg, 2005, 372 p.
4. *Artificial Receptors for Chemical Sensors*, eds. V. M. Mirsky and A. K. Yatsimirsky, Wiley-VCH, 2010, 486 p.
5. R. Parkesh, E. B. Veale and T. Gunnlaugsson, in *Chemosensors: Principle, Strategies, and Applications*, eds. B. Wang and E. V. Anslyn, Wiley Series in Drug Discovery and Development, John Wiley & Sons, Inc. , Hoboken, 2011, pp. 229–252.
6. N. Verma and G. Kaur, in *Comprehensive Analytical Chemistry*, ed. V. Scognamiglio, G. Rea, F. , Arduini and G. Palleschi, Elsevier, Amsterdam, 2016, p Vol. 74, p. 33–71.
7. N. Zaccheroni, F. Palomba and E. Rampazzo, in *Applied Photochemistry: When Light Meets Molecules*, eds. G. Bergamini and S. Silvi, Springer, Cham, 2016, pp. 479–497.
8. Y. Lin, D. Gritsenko, S. Feng, Y. C. Teh, X. Lu and J. Xu, *Biosens. Bioelectron.* 2016, **83**, 256–266.
9. C. Barbara, S. Ewelina and M. Robert, *Med. Chem.*, 2018, **14**, 19–33.
10. H. Sugihara and K. Hiratani, *Coord. Chem. Rev.*, 1996, **148**, 285–299.
11. *Fluorescent Chemosensors for Ion and Molecule Recognition*, ed. A. W. Czarnick, ACS Symposium Series, American Chemical Society, Washington, DC, 1993, 226 p.
12. M. Formica, V. Fusi, L. Giorgi and M. Micheloni, *Coord. Chem. Rev.*, 2012, **256**, 170–192.
13. M. C.-L. Yeung and V. W.-W. Yam, *Chem. Soc. Rev.*, 2015, **44**, 4192–4202.
14. X. Qian and Z. Xu, *Chem. Soc. Rev.*, 2015, **44**, 4487–4493.
15. M. Ahmed, M. Faisal, A. Ihsan and M. M. Naseer, *Analyst*, 2019, **144**, 2480–2497.
16. N. Kwon, Y. Hu and J. Yoon, *ACS Omega*, 2018, **3**, 13731–13751.
17. D. T. McQuade, A. E. Pullen and T. M. Swager, *Chem. Rev.*, 2000, **100**, 2537–574.
18. H. Hisamoto and K. Suzuki, *TrAC, Trends Anal. Chem.*, 1999, **18**, 513–524.
19. H. N. Kim, Z. Guo, W. Zhu, J. Yoon and H. Tian, *Chem. Soc. Rev.*, 2011, **40**, 79–93.
20. V. Singh, P. C. Mondal, A. K. Singh and M. Zharnikov, *Coord. Chem. Rev.*, 2017, **330**, 144–163.
21. A. Juris, V. Balzani, F. Barigelletti, S. Campagna, P. Belser and A. von Zelewsky, *Coord. Chem. Rev.*, 1988, **84**, 85–277.
22. A. E. Curtright and J. K. McCusker, *J. Phys. Chem. A*, 1999, **103**, 7032–7041.
23. Q. Zhao, F. Li and C. Huang, *Chem. Soc. Rev.*, 2010, **39**, 3007–3030.
24. P. Alreja and N. Kaur, *RSC Adv.*, 2016, **6**, 23169–3217.
25. K.-L. Wong, J.-C. G. Bünzli and P. A. Tanner, *J. Lumin.*, 2020, **224**, 117256.
26. M. Schmittel, H.-W. Lin, E. Thiel, A. J. Meixner and H. Ammon, *Dalton Trans.*, 2006, 33, 4020– 4028.
27. R. Zhang, Z. Ye, Y. Yin, G. Wang, D. Jin, J. Yuan and J. A. Piper, *Bioconjugate Chem.*, 2012, **23**, 725-733.
28. S. Khatua and M. Schmittel, *Org. Lett.*, 2013, **15**, 4422–4425.
29. M. Schmittel and H.-W. Lin, *Angew. Chem., Int. Ed.*, 2007, **46**, 893–896.
30. X.-d. Wang and O. S. Wolfbeis, *Chem. Soc. Rev.*, 2014, **43**, 3666–3761.
31. R. Zhang, Z. Ye, G. Wang, W. Zhang and J. Yuan, *Chem. – Eur. J.*, 2010, **16**, 6884–6891.
32. H.-J. Park and Y. K. Chung, *Inorg. Chim. Acta*, 2012, **391**, 105–113.
33. R. Zhang, X. Yu, Z. Ye, G. Wang, W. Zhang and J. Yuan, *Inorg. Chem.*, 2010, **49**, 7898–7903.
34. M. R. Gill and J. A. Thomas, *Chem. Soc. Rev.*, 2012, **41**, 3179–3192.
35. W. Zhang, F. Zhang, Y.-L. Wang, B. Song, R. Zhang and J. Yuan, *Inorg. Chem.*, 2017, **56**, 1309–1318.
36. U. Schatzschneider, J. Niesel, I. Ott, R. Gust, H. Alborzinia and S. Wölfl, *ChemMedChem*, 2008, **3**, 1104–1109.
37. D. Mondal, M. Bar, S. Mukherjee and S. Baitalik, *Inorg. Chem.*, 2016, **55**, 9707–9724.
38. M. E. Padilla-Tosta, J. M. Lloris, R. Martónez-Máñez, A. Benito, J. Soto, T. Pardo, M. A. Miranda and M. D. Marcos, *Eur. J. Inorg. Chem.*, 2000, 741–748.

39. S. Watanabe, S. Ikishima, T. Matsuo and K. Yoshida, *J. Am. Chem. Soc.*, 2001, **123**, 8402-8403.
40. Z. Ye, X. An, B. Song, W. Zhang, Z. Dai and J. Yuan, *Dalton Trans.*, 2014, **43**, 13055–13060.
41. J.-N. Wang, Q. Qi, L. Zhang and S.-H. Li, *Inorg. Chem.*, 2012, **51**, 13103–13107.
42. J. Ru, X. Mi, L. Guan, X. Tang, Z. Ju, G. Zhang, C. Wang and W. Liu, *J. Mater. Chem. B*, 2015, **3**, 6205–6212.
43. F. Chen, F. Xiao, W. Zhang, C. Lin and Y. Wu, *ACS Appl. Mater. Interfaces*, 2018, **10**, 26964–26971.
44. S. Kumar, A. Arora, J. Kaushal, P. Oswal, A. Kumar and P. Kumar, *Inorg. Chem. Commun.*, 2019, **107**, 107500.
45. M.-J. Li, B. W.-K. Chu, N. Zhu and V. W.-W. Yam, *Inorg. Chem.*, 2007, **46**, 720–733.
46. A. S. Abel, A. D. Averin, A. V. Cheprakov, I. P. Beletskaya, M. Meyer and A. Bessmertnykh-Lemeune, *Chemosensors*, 2022, **10,** 79.
47. E. Tfouni, F. G. Doro, A. J. Gomes, R. S. d. Silva, G. Metzker, P. G. Z. Benini and D. W. Franco, *Coord. Chem. Rev.*, 2010, **254**, 355–371.
48. L. Zeng, P. Gupta, Y. Chen, E. Wang, L. Ji, H. Chao and Z.-S. Chen, *Chem. Soc. Rev.*, 2017, **46**, 5771–5804.
49. A.-Q. Jia, L.-M. Shi, F. Wu, Z.-F. Xin and Q.-F. Zhang, *J. Organomet. Chem.*, 2018, **855**, 33–43.
50. C. Wu, F. Irshad, M. Luo, Y. Zhao, X. Ma and S. Wang, *ChemCatChem*, 2019, **11**, 1256–1263.
51. T. E. Brook and R. Narayanaswamy, S*ens. Actuators, B*, 1997, **39**, 195–201.
52. M. M. Collinson, J. Taussig and S. A. Martin, *Chem. Mater.*, 1999, **11**, 2594–2599.
53. R. J. Forster and C. F. Hogan, *c*, 2000, **72**, 5576–5582.
54. S. J. Payne, G. L. Fiore, C. L. Fraser and J. N. Demas, *Anal. Chem.*, 2010, **82**, 917–921.
55. H. Li, F. Liu, S. Sun, J. Wang, Z. Li, D. Mu, B. Qiao and X. Peng, *J. Mater. Chem. B*, 2013, **1**, 4146–4151.
56. Q. Shu, C. Adam, N. Sojic and M. Schmittel, *Analyst*, 2013, **138**, 4500–4504.
57. J. Li, M. Cheng and M.-J. Li, *Analyst*, 2017, **142**, 3733–3739.
58. L. Wang, T. Yao, S. Shi, Y. Cao and W. Sun, *Sci. Rep.*, 2014, **4**, 5320–5320.
59. P. D. Beer, O. Kocian, R. J. Mortimer and C. Ridgway, *J. Chem. Soc., Chem. Commun.*, 1991, 1460–1463.
60. P. D. Beer, O. Kocian, R. J. Mortimer and C. Ridgway, *Analyst*, 1992, **117**, 1247–1249.
61. J.-C. Moutet, A. Popescu, E. Saint-Aman and L. Tomaszewski, *Electrochim. Acta*, 1998, **43**, 2257–2262.
62. M. Schmittel and H. Lin, *J. Mater. Chem.*, 2008, **18**, 333–343.
63. E. Palomares, R. Vilar and J. R. Durrant, *Chem. Commun.s*, 2004, 362–363.
64. E. Coronado, J. R. Galán-Mascarós, C. Martí-Gastaldo, E. Palomares, J. R. Durrant, R. Vilar, M. Gratzel and M. K. Nazeeruddin, *J. Am. Chem. Soc.*, 2005, **127**, 12351–12356.
65. M. K. Nazeeruddin, D. Di Censo, R. Humphry-Baker and M. Grätzel, *Adv. Funct. Mater.*, 2006, **16**, 189–194.
66. P. Comba, R. Krämer, A. Mokhir, K. Naing and E. Schatz, *Eur. J. Inorg. Chem.y*, 2006, 4442–4448.
67. Q.-T. Lin, L.-M. Pei, W.-C. Xu, H. Chao and L.-N. Ji, *Inorg. Chem. Commun.*, 2012, **16**, 104–106.
68. P. Zhang, L. Pei, Y. Chen, W. Xu, Q. Lin, J. Wang, J. Wu, Y. Shen, L. Ji and H. Chao, *Chem. – Eur. J.*, 2013, **19**, 15494–15503.
69. F. Cheng, N. Tang, K. Miao and F. Wang, *Z. Anorg. Allg. Chem.*, 2014, **640**, 1816–1821.
70. Y. Zhang, Z. Liu, Y. Zhang, Y. Xu, H. Li, C. Wang, A. Lu and S. Sun, *Sens. Actuators, B*, 2015, **211**, 449-455.
71. Z.-B. Zheng, S.-Y. Kang, Y. Zhao, N. Zhang, X. Yi and K.-Z. Wang, *Sens. Actuators, B*, 2015, **221**, 614–624.
72. X.-W. Liu, Y. Xiao, S.-B. Zhang and J.-L. Lu, *Inorg. Chem. Commun.*, 2017, **84**, 56–58.

73. Z.-B. Zheng, Q.-Y. Huang, Y.-F. Han, J. Zuo and Y.-N. Ma, *Sens. Actuators, B*, 2017, **253**, 203–212.
74. P. Kumar and S. Kumar, *J. Mol. Struct.*, 2020, **1202**, 127242.
75. F. K. Kálmán, M. Woods, P. Caravan, P. Jurek, M. Spiller, G. Tircsó, R. Király, E. Brücher and A. D. Sherry, *Inorg. Chem.*, 2007, **46**, 5260–5270.
76. P. A. Lay, A. M. Sargeson, H. Taube, M. H. Chou and C. Creutz, *Inorg. Synth.*, 1986, **24**, 291–299.
77. A. Mitrofanov, S. Brandès, F. Herbst, S. Rigolet, A. Bessmertnykh-Lemeune and I. Beletskaya, *J. Mater. Chem. A*, 2017, **5**, 12216–12235.
78. A. M. Brouwer, *Pure Appl. Chem.*, 2011, **83**, 2213–2228.
79. *HypSpec*, **http://www.hyperquad.co.uk/HypSpec.htm**.
80. P. Gans, A. Sabatini and A. Vacca, *Talanta*, 1996, **43**, 1739–753.
81. M. T. Beck and I. Nagypàl, *Chemistry of complex equilibria*, Ellis Horwood, Ellis Horwood, 1990.
82. D. J. Anderson, *Clin. Chem.*, 1989, **35**, 2152.
83. A. A. Granovsky, *Firefly version 8*, **http://classic.chem.msu.su/gran/firefly/index.html.**
84. M. Dolg, H. Stoll, H. Preuss and R. M. Pitzer, *J. Phys. Chem.*, 1993, **97**, 5852–5859.
85. Stuttgart RSC 1997 ECP Basis Set was obtained from the Extensible Computational Chemistry Environment Basis Set Database, as developed and distributed by the Molecular Science Computing Facility, Environmental and Molecular Sciences Laboratory which is part of the Pacific Northwest Laboratory, P.O. Box 999, Richland, Washington 99352, USA, and funded by the U.S. Department of Energy.
86. M. J. Cook, A. P. Lewis, G. S. G. McAuliffe, V. Skarda, A. J. Thomson, J. L. Glasper and D. J. Robbins, *J. Chem. Soc., Perkin Trans. 2*, 1984, 1293–1301.
87. V. Balzani, A. Juris, M. Venturi, S. Campagna and S. Serroni, *Chem. Rev.*, 1996, **96**, 759–834.
88. T. Véry, D. Ambrosek, M. Otsuka, C. Gourlaouen, X. Assfeld, A. Monari and C. Daniel, *Chem. –Eur. J.*, 2014, **20**, 12901–12909.
89. A. Ghosh, B. Ganguly and A. Das, *Inorg. Chem.*, 2007, **46**, 9912–9918.
90. R. Ballardini, G. Varani, M. T. Indelli, F. Scandola and V. Balzani, *J. Am. Chem. Soc.*, 1978, **100**, 7219–7223.
91. M. Meyer, L. Frémond, E. Espinosa, R. Guilard, Z. Ou and K. M. Kadish, *Inorg. Chem.*, 2004, **43**, 5572–5587.
92. B. Geißer and R. Alsfasser, *Eur. J. Inorg. Chem.*, 1998, 957–963.
93. C. e. Queffeĺec, M. Petit, P. Janvier, D. A. Knight and B. Bujoli, *Chem. Rev.*, 2012, **112**, 3777−3807.
94. G. Guerrero, J. G. Alauzun, M. Granier, D. Laurencin and P. H. Mutin, *Dalton Trans.*, 2013, **42**, 12569–2585.
95. P. Péchy, F. P. Rotzinger, M. K. Nazeeruddin, O. Kohle, S. M. Zakeeruddin, R. Humphry-Baker and M. Grätzel, *J.Chem. Soc., Chem. Commun.*, 1995, 65–66.
96. S. M. Zakeeruddin, M. K. Nazeeruddin, P. Pechy, F. P. Rotzinger, R. Humphry-Baker, K. Kalyanasundaram, M. Grätzel, V. Shklover and T. Haibach, *Inorg. Chem.*, 1997, **36**, 5937–5946.
97. P. Bonhôte, J.-E. Moser, R. Humphry-Baker, N. Vlachopoulos, S. M. Zakeeruddin, L. Walder and M. Grätzel, *J. Am. Chem. Soc.*, 1999, **121**, 1324–1336.
98. G. Will, J. Sotomayor S. Nagaraja Rao and D. Fitzmaurice, *J.Mater. Chem.*, 1999, **9**, 2297–2299.
99. A.-M. Andersson, R. Isovitsch, D. Miranda, S. Wadhwa and R. H. Schmehl, *Chem. Commun.*, 2000, 505–506.
100. I. Gillaizeau-Gauthier, F. Odobel, M. Alebbi, R. Argazzi, E. Costa, C. A. Bignozzi, P. Qu and G. J. Meyer, *Inorg. Chem.*, 2001, **40**, 6073–6079.
101. A. Hagfeldt, G. Boschloo, L. Sun, L. Kloo and H. Pettersson, *Chem. Rev.*, 2010, **110**, 6595–6663.

102. K. Hanson, M. K. Brennaman, A. Ito, H. Luo, W. Song, K. A. Parker, R. Ghosh, M. R. Norris, C. R. K. Glasson, J. J. Concepcion, R. Lopez and T. J. Meyer, *J. Phys.l Chem. C,* 2012, **116**, 14837–14847.
103. M. Braumüller, M. Schulz, D. Sorsche, M. Pfeffer, M. Schaub, J. Popp, B.-W. Park, A. Hagfeldt, B. Dietzek and S. Rau, *Dalton Trans.*, 2015, **44**, 5577–5586.
104. M. Braumüller, M. Schulz, M. Staniszewska, D. Sorsche, M. Wunderlin, J. Popp, J. Guthmuller, B. Dietzek and S. Rau, *Dalton Trans.*, 2016, **45**, 9216–9228.
105. P. M. DiGiacomo and M. B. Dines, US 4299943, 1981.
106. G. Guerrero, P. H. Mutin and A. Vioux, *Chem. Mater.*, 2001, **13**, 4367–4373.
107. F. Forato, A. Belhboub, J. Monot, M. Petit, R. Benoit, V. Sarou-Kanian, F. Fayon, D. Jacquemin, C. Queffelec and B. Bujoli, *Chem. – Eur. J.*, 2018, **24**, 2457–2465.
108. D. Geldof, M. Tassi, R. Carleer, P. Adriaensens, A. Roevens, V. Meynen and F. Blockhuys, *Surf. Sci.*, 2017, **655**, 31–38.
109. M. Tassi, G. Reekmans, R. Carleer and P. Adriaensens, *Solid State Nucl. Magn. Reson.*, 2016, **78**, 50–55.